KINETICS OF OXYGEN CONSUMPTION AFTER A FLASH OF LIGHT IN THE LATERAL OCELLUS OF THE BARNACLE

S. POITRY AND H. WIDMER
Experimental Ophthalmology Laboratory, University of Geneva, 22, rue Alcide-Jentzer, 1211 Geneva 4, Switzerland

ABSTRACT Until recently, polarographic methods for measuring the time course of transient changes in the rate of oxygen consumption (ΔQO_2) have been applied only to tissue preparations containing thousands of cells. Here, we describe ΔQO_2 measurements on the lateral ocellus of the barnacle (*Balanus eburneus*) which contains only three photoreceptor cells. The decrement of partial pressure of oxygen (ΔPO_2) elicited by an 80 ms flash of light was measured near the cells with a microelectrode and the ΔQO_2 was calculated from the ΔPO_2 using a model of diffusion with spherical symmetry. As shown by mathematical simulation, the exact shape of the preparation is not crucial for our measurements of the time course of the ΔQO_2. For a given ΔQO_2, the model describes correctly the attenuation of the ΔPO_2 measured at increased distances from the preparation. To know more about the mechanisms controlling the ΔQO_2, we compared it with the electrical response of the photoreceptor cells: both responses have a similar spectral dependence, but only the ΔQO_2 was abolished by a 10-min exposure to 50 μM dinitrophenol or to 3 mM amytal. We conclude that the ΔQO_2 reflects an increase in mitochondrial respiration and that it is initiated by the phototransformation of rhodopsin, as was already found in the honeybee drone retina (Dimitracos and Tsacopoulos, 1985; Jones and Tsacopoulos, 1987).

INTRODUCTION

To study the mechanisms controlling the rate of O_2 consumption (QO_2) in living tissues, it is of considerable importance to measure the time course of transient changes of QO_2 (ΔQO_2). From a general point of view, measurements of transient changes, although technically more demanding than measurements of steady states, offer a major advantage: they reveal temporal relationships between the biological responses measured. For example, in the retina of the honeybee drone, Tsacopoulos et al. (1983) measured the time course of the transient increase in QO_2 induced by a flash of light and compared it with the time course of the associated increase in intracellular Na^+. They observed that this ΔQO_2 returned to baseline faster than Na^+ and this led them to conclude that the ΔQO_2 did not reflect an increase in the rate of Na^+ pumping in that preparation.

The conclusion was surprising (cf. e.g., Rang and Ritchie, 1968) and needed confirmation on other preparations of sensory cells. To study the ΔQO_2, a preparation containing few and large cells has some advantages: the QO_2 response of a single cell is then more likely to be detected and it is thus possible to measure, for example, the effects of injecting substances in a cell. Therefore, we developed a method to measure transient changes of QO_2 in a small cluster of cells, or even a single cell. With that method, we have measured the time course of the ΔQO_2 elicited by a flash of light in the lateral ocellus of the barnacle (*Balanus eburneus*) (Poitry and Widmer, 1986); the ocellus contains only three photoreceptor cells, each ~100 μm in diameter (Gwilliam, 1965; Shaw, 1972).

Here we present the method, and we examine if the light-induced ΔQO_2 originates from mitochondria and if it is initiated by the phototransformation of rhodopsin. The question of the relation between ΔQO_2 and Na^+ pumping will be explored in a subsequent article.

(During the course of this work, Fein and Tsacopoulos have studied the light-induced ΔQO_2 in the single photoreceptor cells of the ventral eye of *Limulus* [Fein and Tsacopoulos, 1988, *a* and *b*]. The method they used to estimate the ΔQO_2 of those cells was the one presented here).

MATERIALS AND METHODS

Preparation

Barnacles (*Balanus eburneus*) were supplied by the Marine Biological Laboratory, Woods Hole, MA, and kept for up to four months at room temperature in a tank filled with commercial seawater. They were maintained under a 12 h dark/12 h light cycle and fed twice a week with zooplankton.

The lateral ocellus, with part of the ocellar nerve and some adjacent tissue, was dissected free from the rest of the animal. The tapetum and some of the surrounding tissue were removed with fine forceps, but the transparent tissue of the corneal side was left intact (see Fig. 1). After dissection, the whole preparation, as viewed under the microscope, was

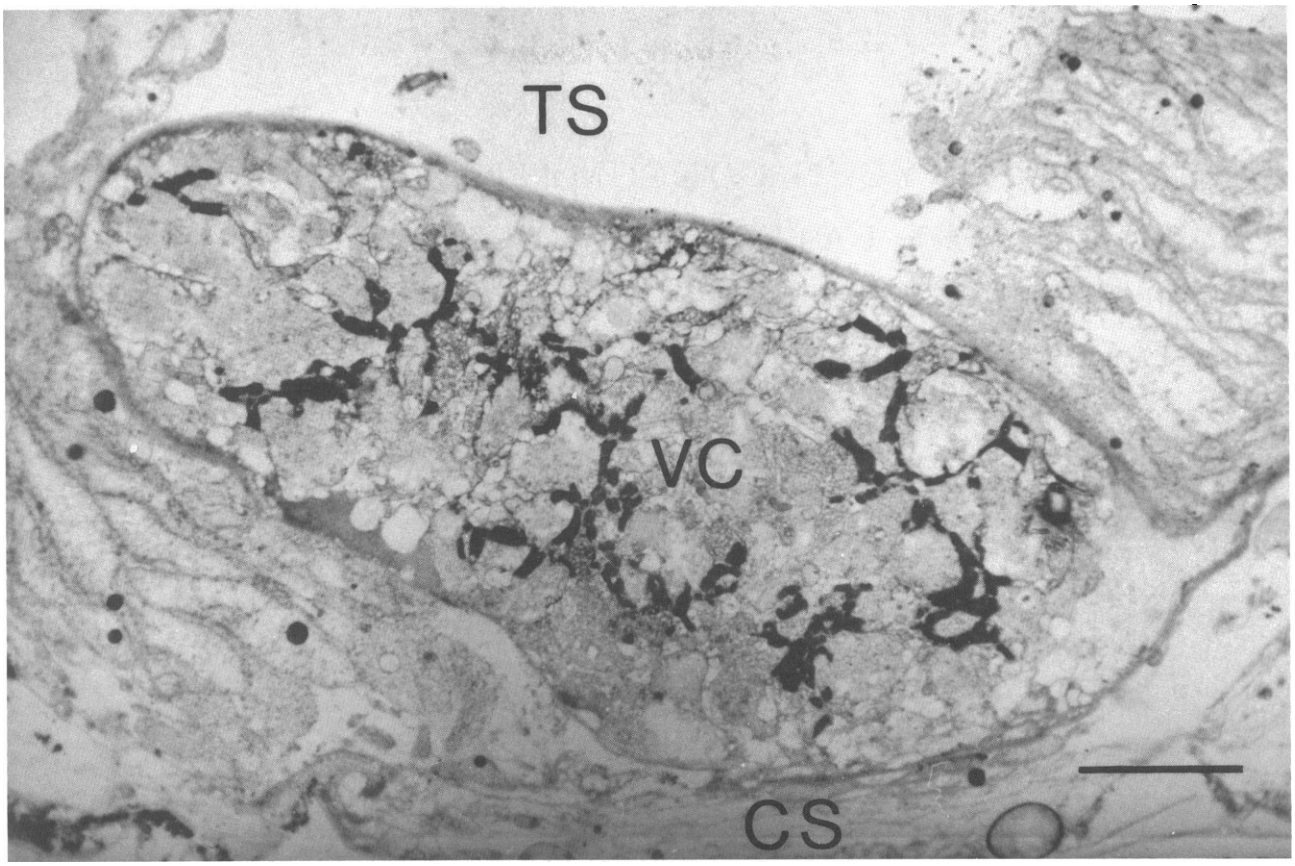

FIGURE 1 Semi-thin section of a preparation after partial dissection. The preparation was stained according to a modification of a method introduced by Cajal (Rålis et al., 1973). Visual cluster (VC); the small darker areas in the cluster are presumably rhabdomeric regions of the photoreceptor cells. Corneal side of the ocellus (CS). Tapetal side (TS). Calibration bar: 20 μm.

about three times larger in diameter than the cluster of photoreceptor and glial cells; attempts at further dissection caused significant and irreversible damage to the cluster, and made it much more difficult to handle.

The preparation was then placed corneal side down on a holder and positioned in the center of a 7-mm deep chamber perfused with air-equilibrated artificial sea water (ASW) (Fig. 2). The holder was designed so as to not impede diffusion of O_2 from the bath to the preparation: it consisted of a small cotton net glued on a silver ring.

Chambers

As discussed in the Theory section, the measurement of the time course of ΔQO_2 required the perfusate to be almost stagnant. We used two different Plexiglas chambers in this study. In the first chamber, the flow rate was kept as low as possible (the perfusate moved <5 mm in 1 min). In the second chamber, the preparation was kept out of the main stream of the perfusate so that the flow rate around it was much smaller than in the first chamber. The bottom of the second chamber was a quartz plate (more details of that chamber will be given in a subsequent paper). Most of the experiments on the validity of the model were done in the first chamber but the results obtained with the second chamber were qualitatively the same. The spectral sensitivity measurements were made using the second chamber.

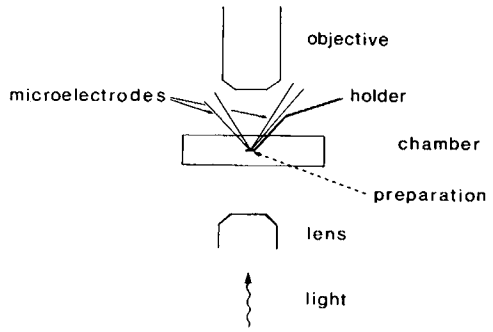

FIGURE 2 Schematic view of the recording arrangement.

Bathing Solutions

The ASW had the following composition: 462 mM NaCl, 8 mM KCl, 10 mM $CaCl_2$, 22 mM $MgCl_2$, 10 mM Tris HCl, pH 7.4. For solutions containing 2,4-dinitrophenol (DNP) (Fluka AG, Buchs, Switzerland), DNP was first dissolved in ethyl alcohol; the final concentration of ethyl alcohol in ASW was <0.1%.

Light Source and Calibration

The light source for viewing and stimulating the preparation was a 150 W xenon arc lamp (XBO 150, Osram GmbH, Munich, West Germany). The light beam passed through a heat filter, interference and/or neutral density filters, and an electromagnetic shutter before being focused on the preparation from below. The flux of the unattenuated beam, measured with a photodiode (OSD 50-1, Centronic Ltd, Croydon, England), was found to be $\sim 4 \times 10^{16}$ photons $\cdot$ mm$^{-2} \cdot$ s^{-1} at the level of the preparation. The transmission factor of the interference filters (Balzers AG, Liechtenstein) was measured with the photodiode placed in the

chamber at the same position as the preparation. All light measurements were made in the quartz bottom chamber.

Microelectrodes and Recording Apparatus

The O_2-sensitive microelectrodes were recess-type Pt electrodes. They were the single-barreled version of the Pt microelectrodes described by Tsacopoulos et al. (1981). Here, there was no need to clamp the polarization voltage because the O_2-sensitive microelectrodes stayed outside the tissue and the stimulus-induced changes in the electrical potential near the tip were negligible (<1 mV). The magnitude of the changes of partial pressure of O_2 (ΔPO_2) was small (<10 mm Hg), so that the stability of the microelectrodes had to be improved: this was achieved mainly by increasing their size. However, since bigger electrodes reduce more O_2, this can affect the PO_2 near the tip and make the measurement less local. The electrodes we used had an inner tip diameter ranging from 1 to 4 μm and a length of recess from 5 to 10 μm; in air-equilibrated ASW, the current ranged from 40 to 150 pA for a −580 mV polarization voltage. Such microelectrodes measured the local PO_2 without affecting it significantly: the current recorded by an O_2-sensitive microelectrode remained unchanged when its tip was brought within <2 μm of that of another O_2-sensitive microelectode. As shown by Tsacopoulos et al. (1981), the current recorded with these microelectrodes is proportional to the local PO_2 over the range 0–700 mmHg. Therefore, we routinely converted the microelectrode current into PO_2 by multiplying it by the PO_2-to-current ratio in the bulk of the air-equilibrated ASW. The electronic equipment used for these recordings was similar to that described by Lehmenkühler et al. (1976) and Tsacopoulos and Lehmenkühler (1977); the high-frequency noise of the signal was removed with a low-pass filter (1 Hz cutoff frequency). When necessary, the position of the microelectrode was measured with a 20 turn potentiometer connected by a rubber O-ring to the fine screw of the micromanipulator (Leitz, Wetzlar, West Germany).

The intracellular electrodes used for recording the membrane potential of the photoreceptor cells were quartz micropipettes (Munoz and Coles, 1987) filled with 3M KCl or K-acetate. They were usually double-barreled because this made them stiffer, and in that case both barrels were connected to the amplifier input. After a slight bevelling, the DC resistance of the electrodes was ~100 MΩ. We found that, with these micropipettes, it was unnecessary to soften the preparation with enzyme before impalement (cf. e.g., Brown et al., 1970).

In most experiments, the signals were amplified and fed into an analog to digital converter where they were digitized at 100 Hz and then sent to a microcomputer (QT, Computer Systems Inc., Lawndale, CA). Responses to stimuli were sampled by the computer and stored on magnetic disks; a sample value was taken every 600 ms for the PO_2 signal, and every 150 ms for the membrane voltage. ΔQO_2 was calculated from the stored PO_2 responses using Eq. (2) (see Theory), and the Fourier transformation and its inverse were performed via a Fast Fourier Transform routine (Brigham, 1974). For all the calculations of ΔQO_2, we used the sine method described by Tsacopoulos and Poitry (1982).

Stimulation Procedures

All the experiments were done at room temperature (22°C). After dissection, we left the preparation for at least 30 min in darkness before starting an experiment. During the experiment and unless otherwise specified, an 80 ms flash of light was presented about every 5 min. For white stimuli, the light source was usually attenuated by 2.4 to 3.6 log units; these intensities were at least 100 times higher than the lowest intensity that could elicit a receptor potential of maximal amplitude in one of the three photoreceptor cells.

In the measurements of spectral sensitivity, the preparation was stimulated at each wavelength (431, 473, 526, and 580 nm) with two flashes of different intensities chosen to produce responses comparable with a criterion response or slightly smaller. The criterion response was less than half a response of maximal amplitude. It was elicited either by a white or a 526 nm flash presented every three flashes so as to monitor possible changes in the sensitivity of the cells. The light intensities used for the measurement of receptor potentials were at least 100 times weaker than for ΔQO_2, because the receptor potential reaches its maximal amplitude at much weaker intensities; as a result, we could reduce the dark interval between flashes to 20 or 30 s. To derive the spectral sensitivity from the measurements, we plotted the amplitude at the peak of the response as a function of the logarithm of the intensity of the light, for each of the four wavelengths tested. We assumed that, in the range of intensities tested for each wavelength, the points would fall on a straight line and we chose by eye the four parallel lines that could best fit the results. From the lines of the fit and from the amplitude at the peak of the criterion responses, we deduced for each wavelength a criterion intensity. The relative sensitivity at a given wavelength was then estimated as the ratio of the criterion intensity for 526 nm to the criterion intensity for that wavelength.

RESULTS

PO_2 Profile and Light-Induced ΔPO_2

The PO_2 measured by an O_2-sensitive microelectrode decreases gradually as the electrode approaches the cluster. This indicates that there is a sustained flux of O_2 from the bath toward the cluster. Measurements of the PO_2 profile near a dark-adapted cluster are shown at the beginning and at the end of the PO_2 record of Fig. 3. Before the recording, the electrode had been placed close to the surface of the cluster; when the electrode was withdrawn in steps of 30 μm, the PO_2 increased at each step, and when the electrode was returned back to the surface of the cluster, the PO_2 decreased to its initial value. As shown at the end of the record, the steady state PO_2 profile remained essentially the same during the experiment. Fig. 3 shows also that a brief flash of light induces a transient drop of the PO_2 (ΔPO_2) that originates from the cluster: for a given stimulus, the ΔPO_2 was larger and faster near the surface of the cluster than away in the bath. Both the ΔPO_2 and the difference between surface PO_2 and bath PO_2 could be irreversibly suppressed by poisoning the preparation with cyanide (not shown here).

To verify that the measured ΔPO_2 reflects a change in the rate of O_2 consumption (QO_2) of the cluster, we studied the effects of perturbations of mitochondrial respiration. For this, we used an uncoupler of oxidative phosphoryla-

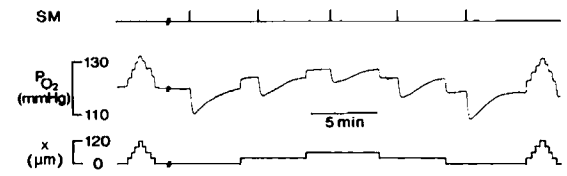

FIGURE 3 Steady-state PO_2 profile and light-induced ΔPO_2s. (*Upper trace*) stimulus monitor. (*Middle trace*) signal from the O_2-sensitive microelectrode. (*Lower trace*) distance of the microelectrode tip from its initial location. Measurements of the PO_2 profile appear as steps on the PO_2 trace and ΔPO_2s as transient downward deflections of the trace. Light stimuli were attenuated by 3.3 log units. After the first measurement of the PO_2 profile, the electrode was withdrawn into the bulk of the bath for calibration (interruption in the trace) and then returned back to the surface of the cluster.

tion, 2,4-DNP, and an inhibitor of mitochondrial respiration, Na-amobarbital (amytal) (Serva, Heidelberg, West Germany). As shown in Fig. 4, exposure to 50 μM DNP caused the PO_2 measured in darkness to drop rapidly to a much lower stable value; in addition, the ΔPO_2 was abolished while the receptor potential was only slightly affected. When the preparation was returned to normal saline, both the PO_2 and the ΔPO_2 recovered gradually, and the recovery was complete after 20 min (not shown here). The effect of 3 mM amytal is shown in Fig. 5. The PO_2 near the cluster in darkness increased and reached a steady value closer, but not equal, to that in the bulk of the bath (Fig. 5 *B*); the increase in PO_2 shown here is the largest we obtained in three preparations. In addition, the ΔPO_2 was abolished after 10 min in amytal. Fig. 5 *A* shows that for the short time the treatment was applied, the membrane and receptor potentials were not affected significantly. The effects on PO_2 and ΔPO_2 were reversible.

From these observations, we concluded that: (*a*) the cluster consumers O_2 in darkness, (*b*) this consumption increases transiently after a flash of light, and (*c*) O_2 in the cluster is replenished by diffusion from the bath. The following section is an attempt to describe the relationship between the measured PO_2 and the QO_2 of the cluster with the mathematics of diffusion.

Theory

The spatial and temporal distribution of the PO_2 in a flowing solution is described by a generalized diffusion equation (see e.g., Eq. [2] in Tsacopoulos et al., 1981). The equation is completed with boundary conditions in which the experimental conditions and the geometry of the whole system are specified. In order to make the problem tractable, the number of relevant parameters should be kept small. This is usually achieved by choosing experimental conditions suitable to the geometry of the preparation, and by making reasonable assumptions about the O_2 consumption of the preparation and the diffusion properties of O_2 in the system.

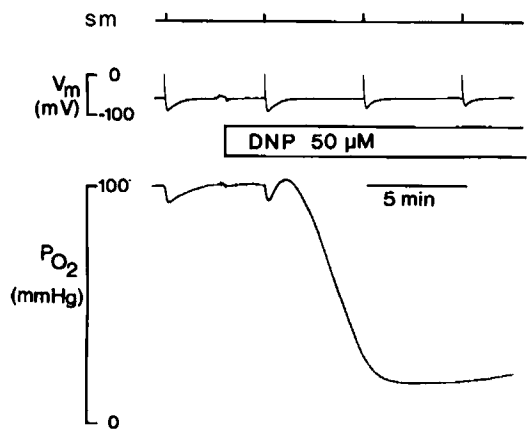

FIGURE 4 Effect of 50 μM DNP. Membrane potential recorded in one photoreceptor cell (*middle trace*) and PO_2 measured simultaneously close to the surface of the cluster (*lower trace*). Stimulus monitor (sm). For each flash, the light was attenuated by 3 log units.

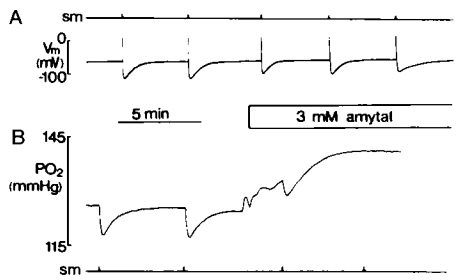

FIGURE 5 Effect of 3 mM amytal. (*A*) membrane potential in one photoreceptor cell. (*B*) PO_2 recorded at the surface of the cluster. Both recordings on the same preparation, but *B* was recorded earlier than *A*. For each flash, the light was attenuated by 3 log units. The PO_2 in the bulk of the bath was 147 mmHg.

Experimental Conditions. The experimental conditions that we chose were as follows: (*a*) the solution was almost stagnant, and (*b*) the ocellus was thoroughly dissected and placed on a net so that O_2 could reach it from all sides (see Methods). The advantage with condition *a* was that the distribution of the PO_2 around the preparation was not disturbed by convective flow: thus, in our measurements, the ΔPO_2 s were maximized, and in our calculations, the convection term of the generalized equation could be dropped. The advantage with condition *b* was that the boundary conditions were then the same over the whole surface of the cluster. We could not actually remove all the connective tissue, but as we shall show, this did not significantly affect our results.

Assumptions. The assumptions we made about the O_2 consumption of the preparation and the diffusion properties of O_2 in the system were: (*a*) O_2 is consumed in the visual cluster only, and not in the fragments of connective tissue; (*b*) at any time, the rate of O_2 consumption is evenly distributed throughout the cluster; (*c*) the diffusion (D) and the solubility (α) coefficients for O_2 are uniform and constant in the cluster (where they have the values D_{sc} and α_{sc}), and in the solution and the connective tissue (where they have the values D_B and α_B). The assumption that the values of D and α in the connective tissue are the same as in the solution is apparently not an oversimplification. We placed an O_2-sensitive microelectrode on the corneal side of the preparation, so that a layer of connective tissue ~250-μm thick remained between the tip of the electrode and the visual cluster. In that position, a flash of light elicited a ΔPO_2 that was similar in amplitude and time course to the ΔPO_2 that we recorded 300 μm away from the cluster, on the other (i.e., dissected) side of the preparation. We could not find numerical values for D and α in seawater at room temperature (22°C) in the literature, and we did not attempt to measure them. Instead, we extrapolated these values from those for water

and for a 0.155 M NaCl solution (Yoshida and Ohshima, 1966; Grote, 1967; Altman and Dittmer, 1971; Vaupel, 1976). The values obtained in this way were: $D_B = 2.1 \times 10^{-5}$ cm^2 · s^{-1} and $\alpha_B = 26$ μl O_2 STP · cm^{-3} · atm^{-1}. As for the values of D_{sc} and α_{sc}, we assumed that they were equal to D_B and α_B, and we examined the consequences of this assumption on the results of the calculations (see below).

Choice of the Geometry. Finally, to calculate the QO_2 of the visual cluster from measurements of PO_2, we needed to choose a geometrical surface to describe its shape. The overall shape of the cluster is variable and irregular, but it can be roughly described as an elongated ellipsoid, or strictly speaking a prolate spheroid, the largest diameter being at most twice as long as the smallest (see Table I). Since the distance from the center of an ellipsoid to a point on its surface varies, a ΔQO_2 occurring uniformly within the ellipsoid will cause a nonuniform ΔPO_2 on its surface, and the formula that relates ΔPO_2 at the surface to ΔQO_2 will depend on the precise position on the surface; however, that position is extremely difficult to measure accurately in a small volume with no fixed shape like the cluster. Since this problem does not arise with a sphere, we examined how the ΔQO_2 deduced from a ΔPO_2 measured on the surface of the cluster is affected when the cluster is described as a sphere instead of an ellipsoid. We found by calculation that if the sphere has the same volume as the ellipsoid, the time course of the calculated ΔQO_2 is only slightly affected: the time needed for the ΔQO_2 to return from its peak to half of it is changed by <7% (see Fig. 12). Therefore, the visual cluster was considered as a sphere in all further calculations and the radius R of the sphere was estimated from the dimensions of the cluster measured under the microscope via the formula: R = (largest half-diameter)$^{1/3}$ × (smallest half-diameter)$^{2/3}$.

The details of the method used to solve the diffusion equation for the spherical model are given in the Appendix. The relation between PO_2 and QO_2 can be described by two equations: one equation relates the steady state PO_2 profile in darkness to the basal QO_2, and the other equation relates the light-induced ΔPO_2 to the transient change of QO_2 (ΔQO_2) that caused it.

Equation relating steady-state PO_2 profile and basal QO_2:

$$P_{sc}(r) = P_B - \frac{Q_{sc}R^3}{3\alpha_B D_B r}, \quad r \geq R, \tag{1}$$

where $P_{sc}(r)$ denotes the steady state PO_2 measured at the distance r from the center of the sphere, P_B is the PO_2 in the bulk of the bath, Q_{sc} is the basal QO_2 per unit volume, R is the radius of the sphere, and α_B and D_B are the solubility and the diffusion coefficients of O_2 in the bath.

Equation relating light-induced ΔPO_2 and ΔQO_2:

$$\Delta Q(t) = F_\omega^{-1}\{H(r, \omega)F_t[\Delta P(r, t)]\}, \tag{2}$$

where t is time, $\Delta Q(t)$ is the time course of the ΔQO_2, $\Delta P(r, t)$ is the time course of the ΔPO_2 measured at the distance r from the center of the sphere, $F_t[\ ]$ is the Fourier transform of the quantity in brackets with respect to time, ω is the frequency conjugate to t, $F_\omega^{-1}\{\ \}$ is the inverse Fourier transform, and $H(r, \omega)$ is the transfer function of the problem.

Dependence on α_{sc}, D_{sc}, and R. The transfer function $H(r, \omega)$ depends on the values of α_{sc}, D_{sc}, and R (see Appendix). These values were known only approximately here because α_{sc} and D_{sc} had not been measured and R could only be roughly estimated from the length and width of the visual cluster measured under the microscope. Therefore, we examined how errors in those values would affect the calculated ΔQO_2. To that end, we calculated the ΔQO_2 of a sphere of radius $R = 100$ μm that causes at its surface a ΔPO_2 like that measured at the surface of the cluster, and we chose for α_{sc} and D_{sc} the same values as for α_B and D_B (see above). Then, we examined the effects of doubling or halving the values of α_{sc} or D_{sc} while keeping unchanged the values of α_B and D_B. From those calculations, we concluded that such errors in the value of D_{sc}

TABLE I

A	*B*	*C*	*D*	*E*	*F*	*G*	*H*
1	72/135	2	0	—	90	2	1*
2	102/170	2	2	283–333	122	1	0
3	100/200	2	2	126–132	126	1	1
4	120/170	2	2	192–199	136	2	2
5	70/140	3	2	96–126	88	2	2*
6	75/143	1	0	—	94	3	1
7	120/220	2	0	—	142	1	1
8	115/135	2	2	96–100	122	1	1
9	80/135	1	1	120	96	1	1*
10	140/205	2	1	233	160	1	1*
11	102/135	1	1	181	112	1	0
12	85/120	2	0	—	96	1	1
13	75/115	1	0	—	86	1	1*
14	75/125	1	1	175	90	1	1
15	75/110	2	1	175	86	2	1
16	68/115	2	1	236	82	2	1*
17	90/130	1	0	—	102	1	1*
18	87/130	3	3	232–251	100	1	1*
19	73/109	2	1	235	84	2	1

A Designation of the preparation.
B Smallest and largest half-diameters of the cluster measured under the microscope (units: micrometer).
C Number of profiles measured for that preparation.
D Number of profiles for which a good fit was found (see text).
E Value (seconds) obtained for r_0 (in micrometers) from the fit with Eq. (1).
F Radius (in micrometers) of the sphere having a volume equal to that of the cluster (this radius was used for computing the ΔQO_2s).
G Number of series of ΔPO_2s recorded for that preparation.
H Number of series of ΔPO_2s for which the ΔQO_2s were the same. The asterisk indicates when it was necessary to assume that the electrode tip was 30 μm away from the surface.

would leave the calculated ΔQO_2 almost unaffected, whereas errors in the value of α_{sc} would cause proportional errors in the amplitude of the calculated ΔQO_2 but have negligible effects on its time course. We also examined the effects of increasing R to 130 μm, or decreasing it to 70 μm, the choice of those values being based on our measurements of the dimensions of the cluster (see Table I). As shown in Fig. 6, such errors in the value of the radius would affect both the amplitude and the time course of the calculated ΔQO_2: a 30 μm reduction of the radius increased the amplitude by 30 to 50% and shifted the return to baseline by 10 to 15 s.

Does the Spherical Model Describe the Results?

We examined this question by measuring the steady state PO_2 profile and the light-induced ΔPO_2 near the cluster.

PO_2 Profile. In the recording shown in Fig. 3, the PO_2 profile was measured twice, once at the beginning and once at the end of the trace. The values of the PO_2 profile measured at the end of the trace are plotted in Fig. 7. In this plot, the location of each measurement is expressed as the distance x between the electrode's tip and its initial position, near the surface of the cluster. The curve is the PO_2 profile obtained with Eq. (1) that gave the closest fit of the results. For the fit, Eq. (1) was rewritten as: $P_{sc}(x) = P_B - A/(r_o + x)$, where r_o is the distance of the initial position from the center of the sphere, and A stands for $Q_{sc}R^3/3\alpha_B D_B$, and we calculated by the method of least mean squares the values of A and r_o. For the profile shown in Fig. 7, the fit was considered to be good and the values found for A and r_o were: $A = 3.87 \times 10^3$ mmHg · μm and $r_o = 126$ μm. Since the lengths of the smallest and of the largest half-diameters of that cluster were 70 and

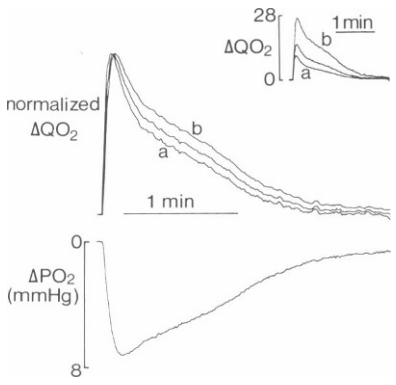

FIGURE 6 Time-course of calculated ΔQO_2: effect of the volume of the sphere. (*Lower trace*) ΔPO_2 recorded near the surface of a cluster of 285 μm by 150 μm. (*Upper traces*) corresponding ΔQO_2 calculated for a radius of 130 μm (*trace a*), 100 μm and 70 μm (*trace b*). ΔQO_2s are normalized at the peak. (*Inset*) ΔQO_2 traces drawn on an absolute scale; units of ΔQO_2 are μl O_2 STP · cm^{-3} · min^{-1}. Each curve is made of 256 points connected by a continuous line.

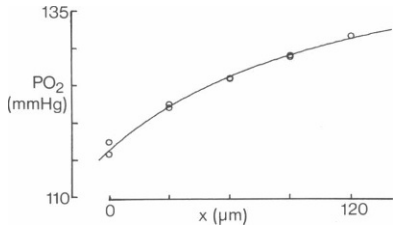

FIGURE 7 PO_2 profile measured (*open circles*) and predicted by the spherical model (*continuous curve*). The experimental values are those obtained at each step of the second series of measurements of Fig. 3.

140 μm, this value of r_o seemed reasonable. For the PO_2 profile measured at the beginning of the trace, the closest fit was not considered to be good: the experimental results were found slightly above the curve at either end of the graph and slightly under the curve at intermediate values (not shown).

Measurements like those of Fig. 3 were repeated on 18 other preparations. The results of the comparison between the PO_2 profiles measured and those predicted by the spherical model are summarized in Table I. For about two profiles in three, the model gave a good fit (i.e., a fit for which there was no systematic deviation between the curve and the data); however, in 9 preparations out of the 13 for which a good fit was found, the values of r_o were much larger than the dimensions of the cluster measured under the microscope. This discrepancy was surprising because we did not expect the initial location of the electrode to be much more than 30 μm away from the surface of the cluster. The best explanation we found was that this test is extremely sensitive to small fluctuations in the signal of the O_2-sensitive microelectrode. This is due to the fact that the fit depends on the difference between the PO_2 measured in the bath (P_B) and the PO_2 measured near the cluster ($P_{sc}[x]$). We found indeed that a 1–2% change in the PO_2 signal could easily lead to a difference of 30 μm in the estimate of r_o or could even prevent us from finding a good fit of the results. Although we calibrated the electrode immediately after each measurement of the PO_2 profile, such fluctuations were still quite likely to occur in the interval between measurement and calibration. Since the results could not be fitted better with an ellipsoidal model, we concluded that this test was too sensitive to experimental errors to provide a definite answer as to the validity of the spherical model. However, this conclusion was not so critical since our aim was to estimate the time course of the light-induced ΔQO_2, and not the basal QO_2.

Light-induced ΔPO_2. A second test of the spherical model was to examine whether it could describe the decrease and the slowing down of the ΔPO_2s measured away from the cluster (see Fig. 3). Since the stimuli were the same, the ΔQO_2s must have been the same; therefore, we examined whether the ΔQO_2s calculated from these ΔPO_2s with the model were the same. We found that, for

this test, fluctuations in the PO_2 signal were not as critical.

The calculation of ΔQO_2 with the model was performed using Eq. (2). For this calculation, we needed to know the radius R of the sphere having the same volume as the cluster, and also the distance r from the center of the cluster to each location where the PO_2 was measured. Both values were experimentally deduced: the value of R was calculated from the dimensions of the cluster measured under the microscope (see Theory) and the value of r was obtained by adding the measured displacement x of the electrode from its initial location, to the distance r_0 from the initial location to the center of the cluster. Since r_0 was not directly measured and since it could not be reliably deduced from the measurement of the PO_2 profiles (see above), we started our calculations by assuming that it was equal to R. The amplitudes of the ΔQO_2s calculated from the ΔPO_2s of Fig. 3 in this way showed a slight systematic deviation. Since some connective tissue might remain between the electrode and the actual surface of the cluster, we examined how the various ΔQO_2s would change if the value chosen for r_0 was larger. We therefore recalculated the ΔQO_2s with a value of r_0 increased by 30 μm, and the resulting ΔQO_2s are shown in Fig. 8: considering the differences in the calculated ΔQO_2s due to fluctuations in the PO_2 signal, we judged that these ΔQO_2s were the same. Indeed, a further increase of the value of r_0 gave larger differences between the curves (not shown).

The results of the comparisons of ΔQO_2s measured at three locations are summarized in Table I for the 19 preparations used in these tests. As already mentioned, it is unlikely that the electrode was initially much more than 30 μm away from the surface of the cluster. Therefore, if the ΔQO_2s were not the same for a value of r_0 equal to R or 30 μm larger, the results of the tests were considered to be negative. In 17 of the 19 preparations, the results of the test were positive in at least one of the series of measurements. The fact that on the same preparation the results of the test were positive in one series of measurements and negative in another cannot be attributed simply to fluctuations of the signal of the microelectrode, because the way in which the ΔQO_2s differed was always the same: at the more distant sites of recording, the ΔPO_2s were larger than expected from the model. We can find two types of experimental errors to explain this effect: (*a*) the preparation might have followed the electrode when it was withdrawn, or (*b*) the electrode was not displaced along an axis passing through the center of the cluster. Errors of type *a* could occur because we brought the electrode into close contact with the preparation before starting the experiment, and errors of type *b* could occur because it was sometimes difficult to judge where the center of the cluster was. Despite these difficulties, and also because we were able to obtain positive results of the test in most preparations, we concluded from this test that the spherical model could be used to estimate the time course of the ΔQO_2 of the cluster.

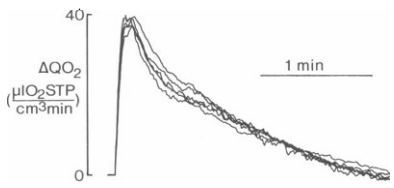

FIGURE 8 Traces of ΔQO_2 calculated from the ΔPO_2s of Fig. 3 with the spherical model. The radius of the sphere was 88 μm and the ΔQO_2s were calculated assuming that the initial location of the electrode tip was 30 μm away from the surface.

Amplitude and Time Course of ΔQO_2. In experiments where the test gave positive results, we measured the time necessary for the ΔQO_2 to return to 10% of its peak, and the average value we found was 105. ± 4.4 s (standard error, $n = 19$). In most cases, the recovery of the ΔQO_2 was apparently monophasic (see Fig. 8). However, in a few cases, ΔQO_2s with two distinct recovery phases were encountered (see Fig. 6); even though the relative magnitudes of the two phases could be affected by errors in the radius chosen for the calculation, the existence of these two phases was unquestionable. The amplitude at the peak of the ΔQO_2 ranged from 4 $\mu l\ O_2 \cdot cm^{-3} \cdot min^{-1}$ to 38 $\mu l\ O_2 \cdot cm^{-3} \cdot min^{-1}$. The variability in the amplitudes was partly due to differences in the intensity of the stimulus (see Fig. 11).

Spectral Dependence of ΔQO_2

To examine whether the ΔQO_2 of the cluster and the electrical response of the photoreceptor cells have a common origin, we compared their spectral dependence.

We found that for brief and moderate stimuli, the time courses of the receptor potential and of the ΔQO_2 were independent of the color. Then we measured the spectral

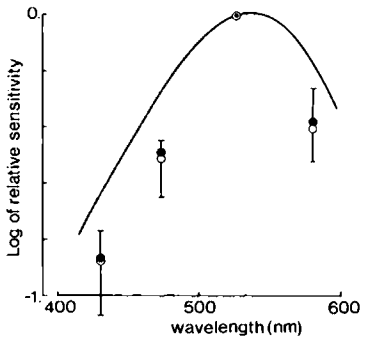

FIGURE 9 Spectral sensitivity of ΔQO_2 (*open circles*) and receptor potential (*filled circles*). The vertical bars are standard deviations; the values at 526 nm being chosen as reference, they have no associated error bars. For the ΔQO_2, measurements were made in four preparations and for the receptor potential, they were made in three photoreceptor cells, each from a different preparation. The solid curve is a Dartnall nomogram (Dartnall, 1953) with peak at 540 nm. The bottom of the chamber used for the measurements was a quartz plate.

dependence of the amplitude at the peak of both responses (see Methods) at four wavelengths (431, 473, 526, and 580 nm). The spectral sensitivity of the cluster for the ΔQO_2 was undistinguishable from that for the receptor potential (Fig. 9). When the data were compared with a Dartnall nomogram with peak at 540 nm (Dartnall, 1953), they were found below the curve on either side of the peak.

For strong and long stimuli, the time course of the receptor potential can show a color dependence: illumination with red light induces a prolonged depolarizing afterpotential (PDA) (Hochstein et al., 1973; Brown and Cornwall, 1975). Fig. 10 *A* shows the receptor potential and the associated ΔQO_2 elicited by a 10 s illumination with blue light. Upon termination of the illumination, the membrane potential hyperpolarized while the ΔQO_2 recovered with an initial rapid phase. In contrast, after a 10 s illumination with red light (Fig. 10 *B*), a PDA was induced and the recovery of the ΔQO_2 showed no rapid initial phase. These effects of red light were terminated with subsequent blue light. Similar results were obtained in two other preparations.

Post-illumination Hyperpolarization and ΔQO_2

Since the ΔQO_2 of the cluster and the electrical response of the photoreceptor cells have a similar spectral dependence, we further explored their possible relationships by measuring them simultaneously at various intensities of white light.

For moderate intensities, the peak amplitude of both the ΔQO_2 and the post-illumination hyperpolarization (PIH; Koike et al., 1971) increased in parallel and linearly with the log of the intensity (Fig. 11). The same result was obtained in ten other preparations. For stronger intensities, the amplitude of the ΔQO_2 and the PIH tended to a maximal value and the responses were prolonged (not shown). The maximal amplitude of the PIH can be quite large (Shaw, 1972); here, it routinely ranged from -50 to -80 mV relative to resting potential. For the brief flashes used here, the PIH appeared at light intensities for which the amplitude of the receptor potential was already maximal.

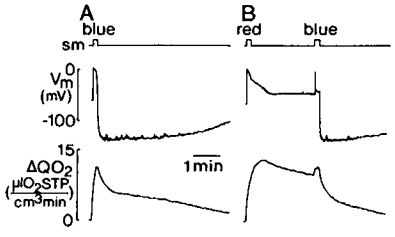

FIGURE 10 Simultaneous measurements of membrane potential (*middle trace*) and ΔQO_2 (*bottom trace*). (*A*) Effect of 10 s illumination with unattenuated blue light (431 nm). (*B*) Effect of 10 s illumination with unattenuated red light (580 nm) followed by 10 s with blue light.

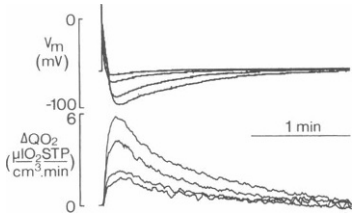

FIGURE 11 Superimposed responses to flashes of increasing intensity. The top trace is the membrane potential recorded in one photoreceptor cell and the bottom trace is the associated ΔQO_2 of the cluster. The responses increased with the intensity of the light. The stimulus was presented at the beginning of each pair of traces and its intensity was doubled each time. For the lowest intensity, the light was attenuated by 2.7 log units.

In addition, the ΔQO_2 and the PIH seemed to depend on mechanisms that recover in parallel from illumination: in most of the preparations used here, when there was no detectable PIH for a given stimulus there was also no detectable ΔQO_2, and both would eventually appear and grow in parallel as the dark period increased.

DISCUSSION

The major aim of this study was to develop a method for measuring the time course of a transient change in the rate of O_2 consumption (ΔQO_2) in a cluster of few cells. This method is similar to that used by Mahler (1978) and by Tsacopoulos and Poitry (1982) in much larger preparations: the ΔQO_2 is calculated from the change in PO_2 (ΔPO_2) measured near the cells with an O_2-sensitive microelectrode, and the formula used in the calculation is obtained by solving the equation of diffusion for a model geometry.

To apply this method to the visual cluster of the lateral ocellus of the barnacle, a prerequisite has been to make O_2-sensitive microelectrodes stable enough to reliably measure ΔPO_2 s of <10 mmHg (see Methods) and to find a simple model to describe the relationship between the ΔQO_2 in the cluster and the ΔPO_2 measured just outside the cluster.

Tests of the Model

In the simple model chosen for the calculation of the time course of ΔQO_2, the visual cluster was considered as a sphere consuming O_2 uniformly.

The assumption that O_2 is consumed uniformly was certainly arbitrary: as discussed below, O_2 is presumably consumed only within the mitochondria. Unfortunately, very little is known about the distribution of mitochondria in the cluster: Krebs and Schaten (1976) reported the presence of large numbers of them in all regions of the three photoreceptor cells, but they didn't mention their presence in glial cells. However, even if the mitochondria are found predominantly in the photoreceptor cells, their uneven distribution may not matter because these cells

extend throughout the cluster and fill half of it (see e.g., Tsacopoulos et al., 1981).

To consider the cluster as a sphere was convenient but inaccurate: the cluster looks like an elongated ellipsoid. However, we found by calculation that approximating the cluster by a sphere rather than an ellipsoid does not introduce systematic errors in the time course of the calculated ΔQO_2, provided the sphere has the same volume as the ellipsoid. Mahler et al. (1985), who measured the ΔQO_2 elicited by a short tetanus in the sartorius muscle of the frog, found that the time constant of the recovery phase of the ΔQO_2 decreased by ~15% when they chose a geometry that better described the shape of the tissue; one reason for that difference may be that, in their first model, the volume they chose for the tissue was not the same as in their second model.

If our model is appropriate, it should give a correct description of the steady state PO_2 and of the ΔPO_2 measured at various distances from the cluster. Unfortunately, the performance of our microelectrodes allowed us to use only the second type of measurements to test the spherical model. From this test, we concluded that the spherical model can be used to estimate the time course of the light-induced ΔQO_2.

Light-induced ΔQO_2

As previously observed in the honeybee drone retina (Tsacopoulos and Poitry, 1982), we found that for moderate light intensities the peak amplitude of the ΔQO_2 increased linearly with the log of the intensity (see Fig. 11), without any appreciable change in the shape of the response. However, we saw here a saturation and a prolongation of the ΔQO_2 at strong light intensities.

The time for the ΔQO_2 to recover to 10% of its peak was 105 s, i.e., about ten times more than in the drone retina (Tsacopoulos and Poitry, 1982). Usually and like in the drone, the ΔQO_2 recovered monophasically. However, in a few cases, the recovery was biphasic, indicating that it may be controlled by two (or more) mechanisms, and the two phases were more apparent with long and intense blue illumination (see Fig. 10). Using our method, Fein and Tsacopoulos (1988*b*) have measured the ΔQO_2 induced by its flashes (i.e., flashes more than 10 times longer than we generally used here) in single photoreceptor cells of the ventral eye of *Limulus:* the ΔQO_2 recovered in about the same time as in barnacle, but usually in two phases, the first one being much faster than that seen occasionally in barnacle.

Spectral Dependence of ΔQO_2 and Receptor Potential

As measured from the ΔQO_2, the spectral sensitivity of the cluster was similar to that of the photoreceptor cells: both were higher at 526 than at 580 or 473 nm. Several authors have already measured the spectral sensitivity of the photoreceptor cells of the barnacle (receptor potential: Stratten and Ogden, 1971; Shaw, 1972; Strong and Lisman, 1978; light-induced current: Brown and Cornwall, 1975): they found that it peaks between 530 and 540 nm and their data, like ours, fell below the Dartnall nomogram used to fit them. In addition, from measurements of the early receptor potential, Minke et al. (1973) concluded that the visual pigment of the lateral ocellus exists in two stable and photointerconvertible states: one state (rhodopsin) absorbs maximally at 532 nm, and the other (metarhodopsin) at 495 nm. These observations suggest that the phototransformation of rhodopsin initiates not only the receptor potential but also the light-induced ΔQO_2.

In the drone retina, Jones and Tsacopoulos (1987) found that the action spectrum of the ΔQO_2 matches that of the receptor potential, and that both spectra deviate only slightly from the absorption spectrum of rhodopsin, which peaks at 446 nm in that preparation. As they pointed out, the fact that the same result is found in preparations with different photosensitivities supports the conclusion that both responses are initiated by the phototransformation of rhodopsin.

Further evidence is obtained with illuminations that shift large amounts of pigment predominantly from one state to the other. In barnacle, red light shifts the pigment from the rhodopsin to the metarhodopsin state, whereas blue light shifts the pigment in the reverse direction (Minke et al., 1973). As we show here, the ΔQO_2 elicited by strong red light (580 nm) was prolonged, while the receptor potential was followed by a prolonged depolarizing afterpotential (PDA: Hochstein et al, 1973; Brown and Cornwall, 1975; Minke, 1986); on the other hand, strong blue light (435 nm) terminated the PDA and sped up the recovery of the ΔQO_2.

In the drone retina, strong blue light (410 nm) prolongs both the receptor potential and the ΔQO_2, an effect that is prevented by the immediate addition of green light (530 nm) (Jones and Tsacopoulos, 1987). These results are equivalent to those obtained in barnacle because, in the drone retina, rhodopsin absorbs maximally at a shorter wavelength than metarhodopsin (Muri and Jones, 1983).

Effects of Metabolic Inhibitors

We have shown that a 10 min exposure to 50 μM DNP or to 3 mM amytal abolished the light-induced ΔPO_2 while the receptor potential was only slightly affected. Since the ΔQO_2 and the receptor potential appear to be both initiated by the phototransformation of rhodopsin (see above), their dissociation by DNP and amytal shows that there are intermediate steps between the absorption of light by the pigment and the ΔQO_2 response. In addition, since both DNP and amytal are known to affect mitochondrial respiration (Slater, 1967), their effect on the ΔQO_2 suggests that the response originates from mitochondria.

As we report here, DNP caused a large decrease in basal PO_2 (i.e., a large increase in QO_2), probably because DNP

uncouples oxidative phosphorylation in the mitochondria. Similar effects of DNP on the basal PO_2 have been observed in slices of drone retina (Tsacopoulos et al., 1988).

Our observation that amytal abolished the ΔQO_2 without suppressing the basal QO_2 is similar to the observations made by other authors. In the drone retina, Dimitracos and Tsacopoulos (1985) found that, for a time of exposure slightly shorter than ours, 3 mM amytal inhibited the light-induced ΔPO_2 and caused a small increase of the basal PO_2. In the perfused rat heart, Nishiki et al. (1979) showed that with 3 mM amytal the ΔQO_2 was greatly reduced and the beating stopped.

Lantz and Mauro (1978) found that exposure to DNP abolished the receptor potential in the lateral ocellus; however, the disagreement with our results is only apparent because they used higher concentrations of DNP (0.1–0.2 mM) and stimulated much more frequently (every 10 s) with longer flashes (1 s). Since DNP uncouples oxidative phosphorylation, their protocol may have caused a faster depletion of the ATP in the cells than ours.

ΔQO_2 and PIH

As we just discussed, the ΔQO_2 seems to originate from the mitochondria and to be initiated, like the receptor potential, by the phototransformation of rhodopsin. We looked for additional similarities between the responses and, as already briefly reported (Poitry and Widmer, 1986), we found that the PIH and the ΔQO_2 increase in parallel as the light intensity increases and that their time courses are similar. These results differ markedly from those found in the drone retina (Tsacopoulos et al., 1983) and in the ventral eye of *Limulus* (Fein and Tsacopoulos, 1988*b*) in which cases the ΔQO_2 recovered more rapidly than the PIH. Since the PIH has been attributed to the electrogenic pumping of sodium (Koike et al., 1971; Brown and Lisman, 1972), we suggest that this pumping and the ΔQO_2 are closely related in the lateral eye of the barnacle. This relationship will be explored in a subsequent article.

APPENDIX

Derivation of Eqs. 1 and 2, and of their Counterparts in the Ellipsoidal Model

We shall derive here the equations describing the relation between the QO_2 of the cluster and the PO_2 measured nearby.

As discussed in Theory, we assume that: (*a*) O_2 is consumed only within the cluster; (*b*) the rate of O_2 consumption, Q, may vary in time, but it remains uniform throughout the cluster at all times; (*c*) O_2 in the cluster is replenished by diffusion from the bath, which acts as an inexhaustible reservoir; (*d*) the local solubility of O_2, α, and the local diffusion coefficient of O_2, D, may not be the same in the cluster and in the bath, but they are constant and uniform throughout both regions. With these assumptions, the distribution of PO_2 in the system is described by the diffusion equation (see e.g., Tsacopoulos et al., 1981).

If the cluster is represented as a sphere of radius R and if its whole surface is in contact with the bath, the mathematical problem has spherical symmetry and the diffusion equation reduces to (see e.g., Crank, 1975):

$$\frac{D_B}{r^2}\partial_r[r^2\partial_r P(r,t)] = \partial_t P(r,t), \quad \text{if } r > R,$$

and:

$$\frac{D_c}{r^2}\partial_r[r^2\partial_r P(r,t)] = \partial_t P(r,t) + \frac{Q(t)}{\alpha_{sc}}, \quad \text{if } 0 < r < R. \quad \text{(A1)}$$

$P(r,t)$ is the PO_2 at the distance r from the center of the sphere and at time t, and ∂_r and ∂_t stand for the partial derivatives with respect to r and to t; all other symbols are defined in Theory.

The boundary conditions of the problem are: (*a*) $P(r, t)$ tends to a fixed value, P_B, at very large distances from the cluster; (*b*) the radial component of the diffusion flux, $-D\alpha\partial_r P(r, t)$, vanishes at the center of the cluster; (*c*) $P(r, t)$ and $-D\alpha\partial_r P(r, t)$ are continuous at the surface of the cluster.

To solve this problem, we split it into two: (*A*) a steady-state problem, and (*B*) a time-dependent problem.

(A) Steady-State Problem. In the steady state, $Q(t) = Q_{sc}$ and $P(r, t) = P_{sc}(r)$. The solution of Eqs. (A1) for the boundary conditions above has been given already by Mueller-Klieser (1984); in our notation, it reads:

$$P_{sc}(r) = P_B - \frac{Q_{sc}R^3}{3\alpha_B D_B r}, \quad \text{if } r \geq R, \quad \text{(A2)}$$

and:

$$P_{sc}(r) = P_B - \frac{Q_{sc}R^2}{3\alpha_B D_B} + \frac{Q_{sc}(r^2 - R^2)}{6\alpha_c D_c}, \quad \text{if } 0 \leq r < R. \quad \text{(A3)}$$

Eq. A2 which gives $P_{sc}(r)$ outside the cluster is Eq. 1 of Theory.

(B) Time-dependent Problem. In the time-dependent problem, we examine how transient departures of Q from its steady-state value will affect P. To solve this problem, we use the method of Fourier transforms (see e.g., Tsacopoulos and Poitry, 1982). First, we assume that Q departs from steady state after time $t = 0$, and we express $Q(t)$ and $P(r, t)$ as

$$Q(t) = Q_{sc} + \Delta Q(t)$$

and:

$$P(r, t) = P_{sc}(r) + \Delta P(r, t), \quad \text{(A4)}$$

where $\Delta Q(t) = 0$, $t \leq 0$, and $\Delta P(r, t) = 0$, $t \leq 0$ and $r \geq 0$. Second, we introduce the new expressions of $Q(t)$ and $P(r, t)$ into Eq. A1: the steady-state terms cancel out and the equations relate now only the transient changes of Q and P. Finally, we apply to the equations a Fourier transformation relative to t and we obtain:

$$\frac{D_B}{r^2}\partial_r[r^2\partial_r\Delta P(r, \omega)] = i\omega\Delta P(r, \omega), \quad \text{if } r \geq R,$$

and:

$$\frac{D_{sc}}{r^2}\partial_r[r^2\partial_r\Delta P(r, \omega)] = i\omega\Delta P(r, \omega) + \frac{\Delta Q(\omega)}{\alpha_{sc}}, \quad \text{if } 0 \leq r < R. \quad \text{(A5)}$$

$\Delta P(r, \omega)$ and $\Delta Q(\omega)$ are the Fourier transforms of $\Delta P(r, t)$ and $\Delta Q(t)$, ω is the variable conjugate to t, and $i = (-1)^{1/2}$.

These manipulations affect only slightly the boundary conditions: the new conditions are obtained from the previous ones by replacing $P(r, t)$ with $\Delta P(r, \omega)$, and P_B with zero. With these new conditions, the solution of Eq. A5 is:

$$\Delta P(r, \omega) = -\Delta Q(\omega)\frac{ER}{i\omega\alpha_{sc}Gr}\exp(\lambda[R - r]), \quad \text{if } r \geq R, \quad \text{(A6)}$$

and:

$$\Delta P(r, \omega) = -\Delta Q(\omega)\frac{[Gr - FR\sinh(\mu r)]}{i\omega\alpha_{sc}Gr}, \quad \text{if } 0 \leq r < R. \quad \text{(A7)}$$

where:

$$E = \mu R\cosh(\mu R) - \sinh(\mu R)$$
$$F = [\lambda R + 1]\alpha_B D_B[\alpha_{sc}D_{sc}]^{-1}$$
$$G = E + F\sinh(\mu R)$$
$$\lambda = [|\omega| + i\omega] / [2|\omega|D_B]^{1/2}$$
$$\mu = [\omega + i|\omega|] / [2|\omega|D_{sc}]^{1/2}.$$

To find an expression for ΔQ, we introduce the function $H(r, \omega)$ that we define as:

$$H(r, \omega) = -\frac{i\omega\alpha_{sc}Gr}{ER}\exp(\lambda[r - R]). \quad \text{(A8)}$$

This allows us to rewrite Eq. A6 as:

$$\Delta Q(\omega) = H(r, \omega)\,\Delta P(r, \omega), \quad \text{if } r \geq R. \quad \text{(A9)}$$

Therefore, $H(r, \omega)$ is the transfer function of the problem and $\Delta Q(t)$ is equal to the inverse Fourier transform of the right-hand side of Eq. A9, as expressed by Eq. 2.

If the cluster is represented as a prolate spheroid instead of a sphere, the mathematical problem loses part of its symmetry and retains only rotation symmetry around the long axis of the spheroid. The PO_2 depends then on two space coordinates instead of one and the complexity of the problem increases accordingly. However, despite this increased complexity, the problem can still be solved with a procedure similar to that used above (for more details see S. Poitry, Ph.D. thesis, in preparation). For simplicity, we shall only give here the expressions relating Q to P outside the cluster.

(A) Steady-state Problem. The steady-state solution of the diffusion equation in spheroidal coordinates for the boundary conditions considered here is:

$$P_{sc}(\xi, \eta) = P_B - J\left[\frac{1}{2K}\log_e\left(\frac{\xi + 1}{\xi - 1}\right) - \frac{1}{3(K - L)}Q_2(\xi)P_2(\eta)\right] \quad \text{(A10)}$$

where:

$$J = Q_{sc}AB^2(A^2 - B^2)$$
$$K = 12\alpha_B D_B(A^2 - B^2)^{3/2}$$
$$L = 36(\alpha_B D_B - \alpha_{sc}D_{sc})AB^2Q_2(\xi_o)$$
$$\xi_o = A(A^2 - B^2)^{-1/2}.$$

A and B are the half-lengths of the major and minor axes of the spheroid, ξ and η are the standard spheroidal coordinates (see e.g., Flammer, 1957), and the functions $P_2(\eta)$ and $Q_2(\xi)$ are the associated Legendre functions of second degree and zero order (Stegun, 1972).

(B) Time-dependent problem. The transfer function $H(\xi, \eta, \omega)$ for a prolate spheroid, with the boundary conditions chosen here, is:

$$H(\xi, \eta, \omega) = i\alpha_{sc}\omega\left\{\sum_{n=0}^{\infty}{}' \frac{d_n S_n^{(1)}(c, \eta)[|\omega|R_n^{(1)}(c, \xi) - i\omega R_n^{(2)}(c, \xi)]}{e_n(f_n + g_n)}\right\}^{-1} \quad \text{(A11)}$$

where:

$$d_n = \alpha_c D_c\int_{-1}^{1} S_n^{(1)}(c, \eta')\,d\eta'$$
$$e_n = \int_{-1}^{1}[S_n^{(1)}(c, \eta')]^2\,d\eta'$$
$$f_n = |\omega|(\alpha_{sc}D_{sc} - \alpha_B D_B)R_n^{(1)}(c, \xi_o) + i\omega\alpha_{sc}D_{sc}R_n^{(2)}(c, \xi_o)$$
$$g_n = i\omega\alpha_{sc}D_{sc}R_n^{(1)}(c, \xi_o)R_n^{(2)}(c, \xi_o)[R_n'^{(1)}(c\xi_o)]^{-1}$$
$$c = (|\omega| - i\omega)(A^2 - B^2)^{1/2}(8D_B|\omega|)^{-1/2}$$

The functions $S_n^{(1)}(c, \eta)$, $R_n^{(1)}(c, \xi)$ and $R_n^{(2)}(c, \xi)$ are the spheroidal wave functions (Flammer, 1957), $R_n'^{(1)}(c, \xi)$ and

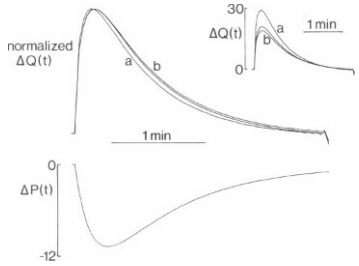

FIGURE 12 Comparison of $\Delta Q(t)$ calculated for an ellipsoid and for a sphere of equal volume. (*Lower Trace*) graph of the function $\Delta P(t)$ used in the calculations. $\Delta P(t)$ was chosen so as to mimic a transient change of the PO_2 measured at the surface of the cluster and it was obtained from the formula: $\Delta P(t) = 20$ mmHg $\cdot$ $[\exp(-t/10\text{ s}) - \exp(-t/50\text{ s})]$. (*Upper traces*) normalized $\Delta Q(t)$ calculated for the sphere and for the ellipsoid ([*a*] on the long axis; [*b*] on the short axis). Each curve was constructed from 64 points. In the ellipsoidal model, the values of the spheroidal wave functions were computed using the method described by Hunding (1983). (*Inset*) same traces drawn on an absolute scale; units of $\Delta Q(t)$ are μl O_2 STP $\cdot$ cm^{-3} $\cdot$ min^{-1}. The radius of the sphere was 100 μm, the largest diameter of the ellipsoid 320 μm, and the smallest 160 μm.

$R_n'^{(2)}(c, \xi)$ are the derivatives of those functions (Flammer, 1957), and the prime sign accompanying Σ indicates that the summation extends only over even values of n.

The relation between $\Delta Q(t)$ and $\Delta P(t)$ at the surface of the cluster in both models is illustrated in Fig. 12.

We are grateful to Drs. M. Tsacopoulos and J. A. Coles for their valuable discussion and constant encouragement, and to Mr. J.-L. Munoz and Mr. P. Perrottet for their expert technical assistance.

This work was supported by the Swiss National Science Foundation grant 3.066-1.84, the Kernen Foundation, and the Sandoz Foundation.

Received for publication 7 March 1988 and in final form 23 May 1988.

REFERENCES

Altman, P. L., and D. S. Dittmer. 1971. Respiration and circulation. Federation of American Societies for Experimental Biology. Bethesda, MD. 17–22.

Brigham, E. O. 1974. The Fast Fourier Transform. Prentice-Hall, Inc., Englewood Cliffs, N.J.

Brown, H. M., and M. C. Cornwall. 1975. Spectral correlates of a quasi-stable depolarization in barnacle photoreceptor following red light. *J. Physiol. (Lond.).* 248:555–578.

Brown, H. M., S. Hagiwara, H. Koike, and R. W. Meech. 1970. Membrane properties of a barnacle photoreceptor examined by the voltage clamp technique. *J. Physiol. (Lond.).* 208:385–413.

Brown, J. E., and J. E. Lisman. 1972. An electrogenic sodium pump in *Limulus* ventral photoreceptor cells. *J. Gen. Physiol.* 59:720–733.

Crank, J. 1975. The mathematics of diffusion. 2nd ed. Clarendon Press, Oxford, U.K.

Dartnall, H. J. A. 1953. The interpretation of spectral sensitivity curves. *Brit. Med. Bull.* 9:24–30.

Dimitracos, S. A., and M. Tsacopoulos. 1985. The recovery from a transient inhibition of the oxidative metabolism of the photoreceptors of the drone (Apis mellifera ♂). *J. Exp. Biol.* 119:165–181.

Fein, A. and M. Tsacopoulos. 1988*a*. Activation of mitochondrial oxidative metabolism by calcium ions in *Limulus* ventral photoreceptors. *Nature (Lond.).* 331:437–440.

Fein, A., and M. Tsacopoulos. 1988*b*. Light-induced O_2 consumption in *Limulus* ventral photoreceptors does not result from a rise in intracellular sodium concentration. *J. Gen. Physiol.* 91:515–527.

Flammer, C. 1957. Spheroidal wave functions. Stanford University Press, Stanford, CA.

Grote, J. 1967. Die Sauerstoffdiffusionskonstanten im Lungengewebe und Wasser und ihre Temperaturabhängigkeit. *Pflüegers Arch. Gesamte Physiol. Menschen Tiere.* 295:245–254.

Gwilliam, G. F. 1965. The mechanism of the shadow reflex in Cirripedia. II. Photoreceptor cell response, second-order responses, and motor cell output. *Biol. Bull. (Woods Hole).* 129:244–256.

Hochstein, S., B. Minke, and P. Hillman. 1973. Antagonistic components of the late receptor potential in the barnacle photoreceptor arising from different stages of the pigment process. *J. Gen. Physiol.* 62:105–128.

Hunding, A. 1983. Bifurcations of nonlinear reaction-diffusion systems in prolate spheroids. *J. Math. Biol.* 17:223–239.

Jones, G. J., and M. Tsacopoulos. 1987. The response to monochromatic light flashes of the oxygen consumption of honeybee drone photoreceptors. *J. Gen. Physiol.* 89:791–813.

Koike, H., H. M. Brown, and S. Hagiwara. 1971. Hyperpolarization of the barnacle photoreceptor membrane following illumination. *J. Gen. Physiol.* 57:723–737.

Krebs, W., and B. Schaten. 1976. The lateral photoreceptor of the barnacle, *Balanus eburneus*. *Cell Tissue Res.* 168:193–207.

Lantz, C. R., and A. Mauro. 1978. Alteration of sensitivity and time scale in invertebrate photoreceptors exposed to anoxia, dinitrophenol, and carbon dioxide. *J. Gen. Physiol.* 72:219–231.

Lehmenkühler, A., H. Caspers, and E. J. Speckmann. 1976. A method for simultaneous measurements of bielectric activity and local tissue PO_2 in the CNS. *Adv. Exp. Med. Biol.* 75:3–7.

Mahler, M. 1978. Kinetics of oxygen consumption after a single isometric tetanus of frog sartorius muscle at 20°C. *J. Gen. Physiol.* 71:559–580.

Mahler, M., C. Louy, E. Homsher, and A. Peskoff. 1985. Reappraisal of diffusion, solubility, and consumption of oxygen in frog skeletal muscle, with applications to muscle energy balance. *J. Gen. Physiol.* 86:105–134.

Minke, B. 1986. Photopigment-dependent adaptation in invertebrates. Implications for vertebrates. *In* The Molecular Mechanism of Photoreception. Stieve, H., editor. Springer-Verlag GmbH & Co. KG, Heidelberg, Berlin. 241–265.

Minke, B., S. Hochstein, and P. Hillman. 1973. Early receptor potential evidence for the existence of two thermally stable states in the barnacle visual pigment. *J. Gen. Physiol.* 62:87–104.

Mueller-Klieser, W. 1984. Method for the determination of oxygen consumption rates and diffusion coefficients in multicellular spheroids. *Biophys. J.* 46:343–348.

Munoz, J.-L., and J. A. Coles. 1987. Quartz micropipettes for intracellular voltage microelectrodes and ion-selective microelectrodes. *J. Neurosci. Methods.* 22:57–64.

Muri, R. B. and G. J. Jones. 1983. Microspectrophotometry of single rhabdoms in the retina of the honeybee drone (Apis mellifera). *J. Gen. Physiol.* 82:469–496.

Nishiki, K., M. Erečinska, and D. F. Wilson. 1979. Effect of Amytal on metabolism of perfused rat heart: relationship between glycolysis and oxidative phosphorylation. *Am. J. Physiol.* 237:C221–C230.

Poitry, S., and H. Widmer. 1986. Kinetics of O_2 consumption following a brief flash of light in the lateral eye of the barnacle, *Balanus eburneus*. *J. Physiol. (Lond.).* 378:65.

Rålis, H. M., R. A. Beesley, and Z. A. Rålis. 1973. Techniques in Neurohistology. Butterworths, London, U.K. 122–123.

Rang, H. P., and J. H. Ritchie. 1968. The dependence on external cations of the oxygen consumption of mammalian non-myelinated fibres at rest and during activity. *J. Physiol. (Lond.)* 196:163–181.

Shaw, S. R. 1972. Decremental conduction of the visual signal in barnacle lateral eye. *J. Physiol. (Lond.).* 220:145–175.

Slater, E. C. 1967. Application of inhibitors and uncouplers for a study of

oxidative phosphorylation. *In* Methods in enzymology. R. W. Estabrook and M. E. Pullman, editors. Academic Press, New York. 48–57.

Stegun, I. A. 1972. Legendre Functions. *In* Handbook of Mathematical Functions (10th printing). M. Abramowitz and I. A. Stegun, editors. National Bureau of Standards. Applied Mathematics Series, vol. 55, Chap. 8, pp 331–353.

Stratten, W. P., and T. E. Ogden. 1971. Spectral sensitivity of the barnacle, *Balanus amphitrite*. *J. Gen. Physiol.* 57:435–447.

Strong, J., and J. Lisman. 1978. Initiation of light adaptation in barnacle photoreceptors. *Science (Wash. DC).* 200:1485–1487.

Tsacopoulos, M., J. A. Coles, and G. Van de Werve. 1987. The supply of metabolic substrate from glia to photoreceptors in the retina of the honeybee drone. *J. Physiol. (Paris).* In press.

Tsacopoulos, M., and A. Lehmenkühler. 1977. A double-barrelled Pt-microelectrode for simultaneous measurement of PO_2 and bioelectrical activity in excitable tissues. *Experientia.* 33:1337–1338.

Tsacopoulos, M., R. K. Orkand, J. A. Coles, S. Levy, and S. Poitry. 1983. Oxygen uptake occurs faster than sodium pumping in bee retina after a light flash. *Nature (Lond.).* 301:604–606.

Tsacopoulos, M., and S. Poitry. 1982. Kinetics of oxygen consumption after a single flash of light in photoreceptors of the drone (Apis mellifera). *J. Gen. Physiol.* 80:19–55.

Tsacopoulos, M., S. Poitry, and A. Borsellino. 1981. Diffusion and consumption of oxygen in the superfused retina of the drone (Apis mellifera) in darkness. *J. Gen. Physiol.* 77:601–628.

Vaupel, P. 1976. Effect of percentual water content in tissues and liquids on the diffusion coefficients of O_2, CO_2, N_2, and H_2. *Pflüegers Arch. Eur. J. Physiol.* 361:201–204.

Yoshida, F., and N. Ohshima. 1966. Diffusivity of oxygen in blood serum. *J. Appl. Physiol.* 21:915–919.